

Estuarine retention of larvae: Contrasting effects of behavioral responses to turbulence and waves

Jessica C. Garwood ^{1,2*} Heidi L. Fuchs ² Gregory P. Gerbi ^{3,4} Elias J. Hunter ² Robert J. Chant ²
John L. Wilkin ²

¹College of Earth, Ocean, and Atmospheric Sciences, Oregon State University, Corvallis, Oregon

²Department of Marine and Coastal Sciences, Rutgers, The State University of New Jersey, New Brunswick, New Jersey

³School of Marine Sciences, University of Maine, Orono, Maine

⁴Physics Department, Skidmore College, Saratoga Springs, New York

Abstract

The intensity of small-scale fluid motions varies among coastal seascapes, which could drive species-specific behavioral adaptations in planktonic larvae. For example, inlets and estuaries typically have stronger turbulence and weaker surface gravity waves than the continental shelf. In the Mid-Atlantic Bight, eastern mudsnails (*Ilyanassa obsoleta*) inhabit inlets and estuaries, whereas threeline mudsnails (*Ilyanassa trivittata*) inhabit the continental shelf. The two species' larvae respond differently to hydrodynamic signals: both hover in calm conditions and sink in response to vorticity, a signal of turbulence, while only shelf snail larvae also sink and swim up in response to accelerations, which can be large under waves. We investigated how these observed larval behaviors and more idealized ones affect retention and settlement in estuaries using numerical experiments. Virtual larvae were released and tracked in a regional model of Delaware Bay and the adjacent shelf. Behaviors that involved downward motions, including vorticity-induced behaviors, helped concentrate larvae near the bottom and enhanced retention in the bay. In contrast, behaviors that involved upward motions, including acceleration-induced behaviors, promoted export onto the shelf. Compared to neutral buoyancy, the vorticity-induced behaviors also conferred longer residence times in the bay, higher settlement probabilities, and shorter pelagic larval durations, all of which would be advantageous to estuarine species. This integration of larval observations with simulations provides evidence that behavioral responses to coastal physics can reduce larval mortality by enhancing retention and settlement in native seascapes.

Many benthic invertebrate species have planktonic stages whose dispersal is governed by the interaction of ocean currents and larval behaviors such as swimming or sinking

(e.g., Metaxas 2001; Levin 2006; Paris et al. 2007), which can change in response to both fluid properties and fluid motions (e.g., Welch and Forward 2001; Daigle and Metaxas 2011; DiBacco et al. 2011). Turbulent motions can alter larval behavior either by reorienting larvae (Clay and Grünbaum 2010; Roy et al. 2012) or by inducing active diving (Wheeler et al. 2015; Fuchs et al. 2015b), passive sinking (Fuchs et al. 2010), and changes in swimming effort (Fuchs et al. 2015a, 2018). In some echinoderm species, acute exposures to turbulence can also increase settlement by triggering early competency (Gaylord et al. 2013; Hodin et al. 2015). Larval responses to turbulence vary between species and can be tuned to the signal intensity in their native environment (Fuchs et al. 2018; Hodin et al. 2020). This variation in behavior can concentrate larvae at different depths (Fuchs et al. 2010, 2018), exposing them to distinct ocean currents that would result in unique larval transport pathways (Pineda and Reynolds 2018). However, turbulence-induced behaviors have been explored primarily in the laboratory, and their effects on species-specific larval transport have not yet been

*Correspondence: jessica.garwood@oregonstate.edu

This is an open access article under the terms of the Creative Commons Attribution License, which permits use, distribution and reproduction in any medium, provided the original work is properly cited.

Additional Supporting Information may be found in the online version of this article.

Author Contribution Statement: All authors contributed to the study's conception, technical and scientific development, and execution in a truly collaborative effort. JCG performed and analyzed the numerical experiments, led development of the analysis framework, and wrote the manuscript; HLF led project conceptualization, development of the behavioral and growth models, and planning of numerical experiments; GPG and EJJ led development of the nested model and implementation of hydrodynamic simulations; EJJ led development of ROMSPATH; RJC guided the Péclet and estuarine circulation analyses; and JLW developed the outer model domain. All authors provided input on analysis and editing.

assessed in the context of time- and space-varying ocean currents.

Coastal hydrodynamics create seascapes of fluid motions that are geographically unique in their intensity and depth structure (Lentz and Fewings 2012; Fuchs and Gerbi 2016). This spatial variation creates distinct hydrodynamic environments for non-overlapping populations, potentially resulting in species-specific adaptations and larval behaviors (Fuchs et al. 2018; Hodin et al. 2020). Mollusk larvae likely sense water motions using their statocysts and respond behaviorally to vorticity-induced body tilting and acceleration (Wheeler et al. 2015; Fuchs et al. 2018). Vorticity signals are specific to turbulence, whereas acceleration signals can also be generated by surface waves. The overall behavior and dispersal of mollusk larvae could, therefore, be modulated by the relative intensity of both turbulence- and wave-induced signals within their environment.

In the Mid-Atlantic Bight, two congeneric mudsnail species occupy distinct seascapes and exhibit distinct larval responses to fluid motions generated experimentally (Fuchs et al. 2018). Eastern mudsnails (*Ilyanassa obsoleta*) inhabit inlets and estuaries, whereas threeline mudsnails (*Ilyanassa trivittata*) inhabit the continental shelf. Competent larvae of both species hover in calm conditions, swimming with no net vertical velocity, but react increasingly to fluid motions above a threshold value by intermittently retracting their velum and sinking passively. Intermittent sinking is triggered by vorticity in both inlet and shelf mudsnails, and by acceleration in shelf snail larvae (Fuchs et al. 2018). When not sinking passively, intensifying vorticity causes body tilting and weak *downward* velocities due to gyrotactic sinking, while intensifying acceleration induces shelf larvae to swim *upward* more actively (Fuchs et al. 2018).

The distinct behaviors of mudsnail larvae could promote retention and settlement in their native habitats. Turbulence-induced sinking could increase opportunities for settlement of both species by concentrating larvae near the bed (Fuchs et al. 2007, 2013) while also increasing transport toward shallow-water adults habitats via tidal asymmetries in mixing (Simpson et al. 1990; Jay and Musiak 1994; Pringle and Franks 2001), benthic streaming (Fujimura et al. 2014; Morgan et al. 2017), and in the case of inlet mudsnails, mean estuarine landward flows at depth (Geyer and MacCready 2014). Upward swimming in response to wave accelerations could limit the offshore dispersal of shelf snail larvae by increasing shoreward transport by Stokes drift, which is strongest at the surface (Monismith and Fong 2004; Fuchs et al. 2018). In contrast, a response to accelerations would be of little use to larvae in estuaries where accelerations generated by waves and turbulence are of similar magnitude (Fuchs and Gerbi 2016) and mean surface currents typically flow out of the estuary (Geyer and MacCready 2014).

Here we investigate how empirical larval behaviors affect retention and settlement in estuaries using a regional numerical model of the Delaware Bay and the adjacent shelf.

Delaware Bay hosts non-overlapping populations of both mudsnail species: inlet mudsnails occupy mudflats, while shelf mudsnails are limited to the deeper waters near the mouth of the bay. We used six different empirical and generic behaviors and assessed their fitness by quantifying the time required for virtual larvae to reach competency and/or settle (treating time to settlement or death as the effective pelagic larval duration, PLD), their residence time in the bay, and the percentage of larvae that settled. We also used our numerical simulations and simple models of tidal boundary layers to evaluate conditions where behavior can overcome tidal mixing and enable larvae to concentrate near the seabed. All results in this study are derived from simulations; we therefore omit qualifying larvae as *virtual* or *modeled* and instead specify when observations are used for comparison or to inform our simulations.

Methods

Study area

Delaware Bay is a relatively wide estuary located on the Northeast Shelf of the United States at the border between New Jersey and Delaware, primarily fed by the Delaware river. The estuary has semidiurnal tides with a tidal range of ~ 1.5 m at the mouth and tidal velocities reaching 1.5 m s^{-1} . Time-averaged velocities in the channel are into the bay at depth and out of the bay at the surface (e.g., Geyer and MacCready 2014), though time-averaged velocities on the flats can often be out of the bay at all depths. Significant wave heights are typically less than 0.2 m, but because Delaware Bay has a large fetch, strong winds can occasionally ($< 10\%$ of the time) generate waves with significant wave heights up to 2 m (Chen et al. 2018; Pareja-Roman et al. 2019).

Model setup

Circulation and surface waves in and around Delaware Bay were simulated using the Regional Ocean Modeling System (ROMS; Shchepetkin and McWilliams 2005) and Simulating WAVes Nearshore (SWAN; Booij et al. 1999; Ris et al. 1999) models, respectively (see *Supplemental Method S1* and model configuration files available online; Gerbi et al. 2022a, 2022b). The model configuration uses a pair of structured grids (Fig. 1a) that capture Delaware Bay at high resolution and the Mid-Atlantic Bight region at moderate resolution. The outer-domain model, dubbed *Doppio* (López et al. 2020), extends from Cape Hatteras, NC, to Halifax, Canada, with a horizontal grid resolution of 7 km. *Doppio* is a mature model used for both process studies and data assimilative regional analyses (Levin et al. 2018, 2019; Wilkin et al. 2018; López et al. 2020). The inner-domain model, dubbed *SnailDel*, covers Delaware Bay and the adjacent shelf at 1-km resolution (Hunter et al. 2021). Both grids have 40 terrain-following vertical levels stretched to better refine surface and bottom boundary layers. When ROMS runs, the grids are two-way coupled and exchange information at the *SnailDel* contact points on every

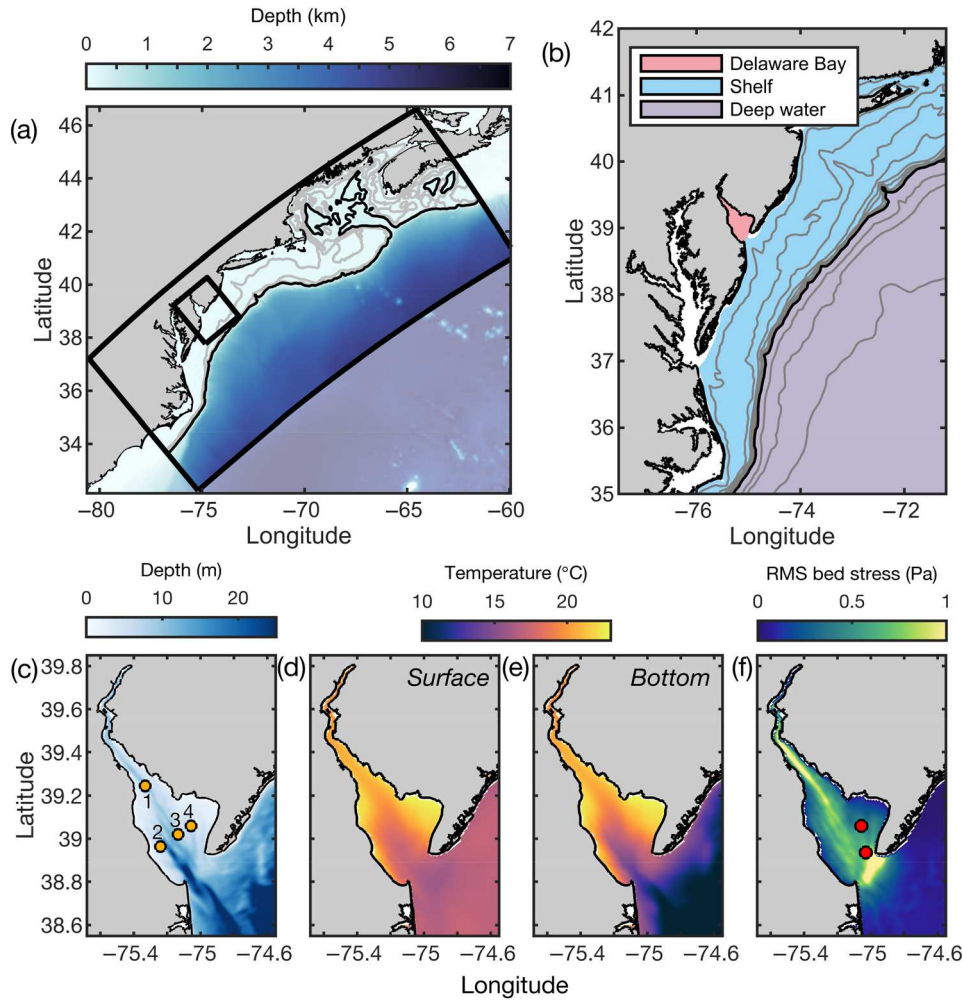


Fig. 1. Model grid domain with (a) local bathymetry and (b) regions considered in this study. The black rectangles show the outer and inner grids, while the solid colors show Delaware Bay (red), the Mid-Atlantic Bight/shelf (blue), and deep waters (purple). Isobaths are shown in gray every 50- and 20-m on the shelf in (a) and (b), respectively, and every 1000-m in deep waters. The shelfbreak is defined by the 200-m isobath (black line). Delaware Bay (c) bathymetry, average (d) surface and (e) bottom temperature during the 2010 releases, and (f) root mean square (RMS) of the bed shear stress over one M2 tidal cycle on April 27, 2010 (spring tide). The yellow dots in (c) show the four larval release sites, while the red dots in (f) show where larval depth distributions were extracted (e.g., Fig. 6).

model time step. Turbulence characteristics were computed using the *k-kl* parameterization (Umlauf and Burchard 2003), and wind-driven wave breaking (whitecapping) was subsequently included using significant wave heights computed with SWAN (Gerbi et al. 2015; Thomson et al. 2016). The ROMS and SWAN simulations cover the period from June 2009 to December 2015. Output was saved every 12 min—an interval that captures circulation and turbulence variability adequately for the subsequent larval transport simulations.

Virtual larval tracking

Larval growth, behavior, and transport were modeled using ROMSPATH (Hunter 2021; Hunter et al. 2021). This offline particle-tracking software builds on the heritage of LTRANS (North et al. 2008) but includes several improvements and added

features necessary for this study (Hunter 2021; Hunter et al. 2021; *Supplemental Method S2*). Larvae were modeled as individual particles transported throughout the domain, and the immediate larval environment was assessed every minute by linearly interpolating hydrodynamic model output to larval positions. Details of physical transport are described in the supplement. Hydrodynamic model outputs were also used to determine larval behaviors (vorticity and acceleration), to compute larval growth (temperature), and to quantify when larvae could settle (bottom shear stress), as described in the following sections.

Behavior signals

Mudsnail larvae change their behavior in response to vorticity ζ and/or acceleration α . We assumed waves were linear, so vorticity was generated only by turbulence, whereas

acceleration was generated by both turbulence and waves. We used the horizontal components of vorticity and acceleration because mollusk larvae respond to rotation only when it changes their orientation relative to gravity, and they respond more to horizontal than vertical acceleration (Fuchs et al. 2015a, 2018).

Our behavior models used vorticity and/or acceleration computed stochastically from modeled dissipation rates and surface wave spectra (details in *Supplemental Method S3*). Prior to input into ROMSPATH, the variances associated with turbulence-induced vorticity ($\sigma_{\zeta_x}^2 = \sigma_{\zeta_y}^2$; Supplementary Eq. S1) and acceleration ($\sigma_{a_x}^2 = \sigma_{a_y}^2$; Supplementary Eq. S2) were calculated from model dissipation rates (ROMS output), while the variances associated with wave-induced acceleration ($\sigma_{a_x}^2$ and $\sigma_{a_y}^2$; Supplementary Eq. S3) were calculated from model surface wave spectra (SWAN output). To estimate the vorticity and acceleration perceived by larvae, the variances of these signals were interpolated to larval positions at each time step in ROMSPATH and then used to rescale random variables generated from Laplace and normal distributions (with zero mean) representing turbulence and surface waves, respectively. Because larvae sense accelerations from both turbulence and surface waves, accelerations from the two sources were added in each horizontal (x and y) dimension to give the instantaneous total accelerations. Finally, we used vector sums of the two horizontal components of vorticities or total accelerations to determine the instantaneous signals. The summed vorticity and total acceleration signals could have positive or negative signs, but only their magnitudes were used to infer behavior.

Behavior models

Larval vertical velocity ultimately reflects a combination of gravity-induced sinking, propulsion, fluid forces on the body, and vorticity-induced body rotation (e.g., Fuchs et al. 2015a, 2015b, 2018). For this study, we omitted the underlying mechanics and modeled velocity directly (Fig. 2). We considered four endmember behaviors: passive sinking, hovering, ascending, and gyrotactic sinking. The passive sinking behavior represents the larva retracting its velum and sinking at a size-dependent terminal velocity (Fig. 2b). The other three behaviors all represent cases in which the larvae attempt to swim upward with varying effort. In hovering, the larval behavioral velocity is zero, and in ascending, the larval behavioral velocity is upward. The gyrotactic sinking behavior occurs in turbulence when fluid vorticity rotates the larva away from its normal vertical orientation. When reoriented, the larva’s upward propulsive force is insufficient to counteract the gravitational force, resulting in a downward velocity (e.g., Fuchs et al. 2018). The larva’s swimming effort and energy expenditure can be identical when hovering or sinking gyrotactically, but they must increase to ascend.

Our behavioral model was based on laboratory observations (Fuchs et al. 2018) of larval responses to vorticity and acceleration (Fig. 2; *Supplemental Method S4*). One class of larvae

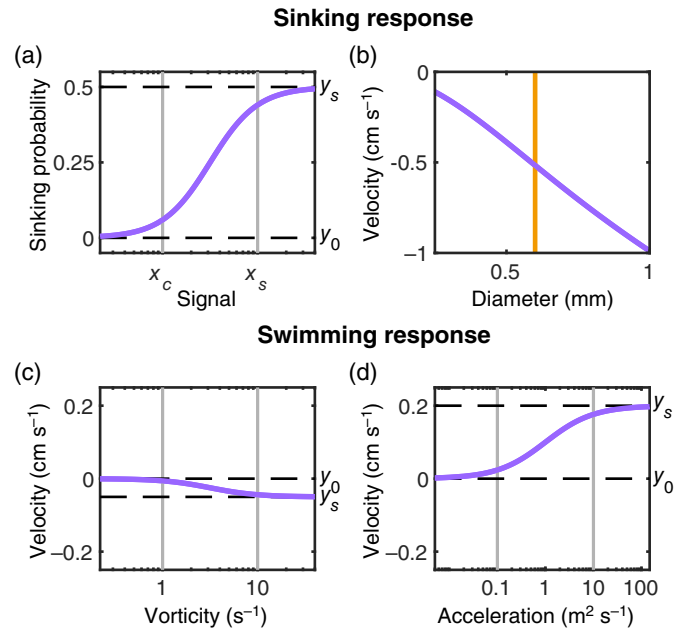


Fig. 2. Larval behavior models. (a) Probability of sinking as a function of signal strength and (b) larval sinking velocity (cm s⁻¹) as a function of diameter (mm). The yellow line shows size at the onset of competency. Larval vertical velocities in response to (c) vorticity (s⁻¹) and (d) acceleration (m² s⁻¹). Dashed lines show values in still-water (y_0) and at saturation (y_s); gray lines show the critical (x_c) and saturation (x_s) signal strengths. Note that the velocity range in (b) is twice that of (c) and (d).

responded only to vorticity—representing the inlet snail, a second responded only to acceleration, and a third responded to both signals—representing the shelf snail. For larvae that responded to both acceleration and vorticity, responses were determined independently for each signal (Fig. 2) and then were combined into a single behavioral velocity as described in the supplement. We contrasted these three empirically based behaviors with three additional behaviors: constant swimming up ($w_s = 0.05$ cm s⁻¹), constant swimming down ($w_s = -0.05$ cm s⁻¹), and constant hovering or neutral buoyancy ($w_s = 0$ cm s⁻¹).

Growth and settlement

To focus our investigation on the effects of larval behavior, we used the same temperature-based growth model G for both snail species (salinity has a much smaller effect; Scheltema 1965, 1967; Fuchs et al. 2018):

$$G = b_0 + b_1 T + b_2 T^2, \tag{1}$$

where T is temperature in °C and the parameters $b_0 = -29.8$ μm d⁻¹, $b_1 = 3.86$ μm d⁻¹°C⁻¹, and $b_2 = -0.07$ μm d⁻¹°C⁻² are based on observations (Scheltema 1967; Fuchs et al. 2018). Larval diameters were set to 250 μm at release (Scheltema 1965; Pechenik 1978) and were updated at every time step. Larvae with diameters ≥ 600 μm were considered

competent until they reached 1000 μm , at which point they were deemed lost (Scheltema 1967).

Larval settlement depends on a variety of biological and physical factors, including substrate type, cues from conspecifics, and microhabitats (e.g., Scheltema 1961; Abelson and Denny 1997). Because our hydrodynamic model omits such complexity, we identified settlement opportunities using a larva's proximity to the seabed and the strength of the bed shear stress τ (e.g., Crimaldi et al. 2002). Larvae were considered settled if at any time following competency, they were within 3 cm of the seabed—a distance which could be covered by constant swimmers in one time step—and τ was less than the critical shear stress for incipient motion of sediment grains with comparable size and density (Soulsby and Whitehouse 1997).

Experimental design

We modeled larval transport using temperature-timed releases over six model years (2010–2015). Releases were triggered when bottom water temperatures warmed to 8°C, which is in the range of temperatures inducing spawning in both mudsnail species (Scheltema 1965, 1967; Pechenik 1978). The larval releases in Delaware Bay occurred in late winter to early spring, with onset dates ranging from February 28 to April 8 (Supplementary Table S2). For every behavior and year simulated, virtual larvae were released 0.25 cm above the seabed from four representative locations in the Delaware Bay (Fig. 1c). Each year, larvae were released from all four locations within an average of 5 ± 2 d, with a maximum offset of 8 d in 2012.

To limit the influence of tides and specific weather events, larvae were released hourly for 10 days at a rate of 80 larvae per hour (a total of 19,200 larval particles per behavior per site per year). The number of larvae per release was chosen to consistently give a small fraction of unexplained variance ($FUV < 0.05$) after 60 d, following Simons et al. (2013). Larvae were tracked for 60 d, or until they exited the model domain. Although *I. obsoleta* larvae reach competency in only 10–24 d in warm laboratory conditions (18–25°C; Scheltema 1967), simulated larvae encountered more realistic, colder temperatures and needed 35–50 d to reach competency. Settlement and size-prescribed death were applied in post-processing.

Analyses

Output summary and code to reproduce the analyses presented in this manuscript have been archived online (Garwood et al. 2022). In our analyses, larvae were grouped based on whether they became competent and settled, became competent but did not settle, or did not become competent and therefore could not settle. The age at settlement was used as the effective pelagic larval duration. For larvae that never settled, the pelagic larval duration was taken to be the time to reach the maximum size or 60 d, whichever came first.

Expecting larvae to settle in the environments where they spent most time, we estimated larval residence time in three major seascapes as well as within smaller regions of Delaware Bay. Seascapes were delineated using three polygons: inside Delaware Bay, the continental shelf (water depths between 10 and 200 m), and deep water (water depths > 200 m) (Fig. 1b). Inside Delaware Bay, we also evaluated residence time within individual SnailDel grid cells, dubbed *grid-cell polygons*. Larval residence time RT within a seascape or grid-cell polygon was computed from the hourly ROMSPATH output and was defined as the total time spent by an individual larva i in a polygon P , including times following exit and re-entry into the polygon:

$$RT = \Delta t_{\text{out}} \times \sum_{i=1}^n \sum_{t=t_1}^{t_2} [(\text{lat}_{i,t}, \text{lon}_{i,t}) \in P], \quad (2)$$

where t is a time step between t_1 and t_2 , and Δt_{out} is the time interval between output (1 h). This formulation assumes that larvae remained within a single polygon for the entire 1-h time step.

To investigate how general patterns of dispersal and settlement related to the prescribed behaviors, our analyses pooled all releases in all years for a given behavior. Because of large sample sizes, our interpretations focus not on the statistical significance of the differences, but on their magnitude and potential biological significance (White et al. 2014b).

Tidal boundary layer model

To help interpret results of our numerical experiments, we used simple models to quantify the relative influence of tidal mixing and behavior on larval depth. Using empirical models of bottom boundary layers (detailed in *Supplemental Method S5*; Hinze 1975; Trowbridge 1992; Chant et al. 2007), we quantified the Péclet number $Pé$ and compared the magnitudes of larval and turbulent vertical velocities, w_s and w' respectively. The Péclet number relates the mixing timescale to the advective timescale (e.g., Ross and Sharples 2004; Ross 2006):

$$Pé = Hw_s/K_z, \quad (3)$$

where H is a characteristic length scale—we use the height of the boundary layer, w_s is the larval behavioral velocity magnitude (swimming or sinking), and K_z is the vertical eddy diffusivity. This non-dimensional number is a useful indicator of whether larval vertical positions are controlled by larval behavior ($Pé \gg 1$) or by turbulent mixing ($Pé \ll 1$). The ratio of velocity magnitudes (w_s/w')—akin to the motility number defined in Gallagher et al. (2004) but focusing on the vertical dimension—has a similar interpretation to $Pé$ but ignores the mixing length scale and therefore reflects the ability of larvae movements to overcome turbulence at a given depth.

The vertical structure of $P\epsilon$ and w_s/w' in the bottom boundary layer was estimated for larvae that respond to vorticity only and for constant-swimming larvae. To assess all possible responses to vorticity, we considered gyrotactic sinking and passive sinking separately. We computed vorticity from its relationship with dissipation rate (Supplementary Eq. S1), which was specified in the simple model along with the vertical eddy diffusivity. In contrast to Gallagher et al. (2004), our computation of w_s/w' did not rely on average quantities, but instead on resampling empirical probability density functions of larval and turbulent velocities. The tidal channel and flats were modeled separately for periods of both weak and strong mixing, which were set by the first and third interquartile values, respectively, of the bed shear stress when larvae were in each location: $\tau = 0.15$ and 0.75 Pa in the channel and $\tau = 0.1$ and 0.5 Pa on the flats (red dots; Fig. 1f).

Results

Though all behaviors led to a similar percentage of larvae becoming competent, there was considerable variation in the percentage of larvae that settled, which was influenced by

their location at competency. For most behaviors, ~85% of larvae became competent (Fig. 3a). Larvae that constantly swam up or down were notable exceptions, as more than 99% of these larvae reached competency (Fig. 3a). Of the behaviors tested, constant downward swimming and the response to vorticity enabled the most settlement. More than half of the larvae settled if they exhibited *any* downward velocities, compared to only 40% for neutrally buoyant larvae and 2% for up-swimming larvae (Fig. 3a).

Spatial patterns of competency and settlement

Overall, the behaviors prescribed to larvae released in Delaware Bay determined their dispersal throughout the Mid-Atlantic Bight (Supplementary Fig. S2). Once larvae exited the bay, south-flowing alongshore currents advected them toward Cape Hatteras, where they were sometimes entrained to deep waters by the Gulf Stream (Supplementary Fig. S2). Larvae that exhibited some downward motions—either constantly or in response to vorticity—primarily became competent in Delaware Bay, although the discrepancy between the percentage of larvae that became competent in the bay and on the shelf decreased when a response to acceleration was introduced

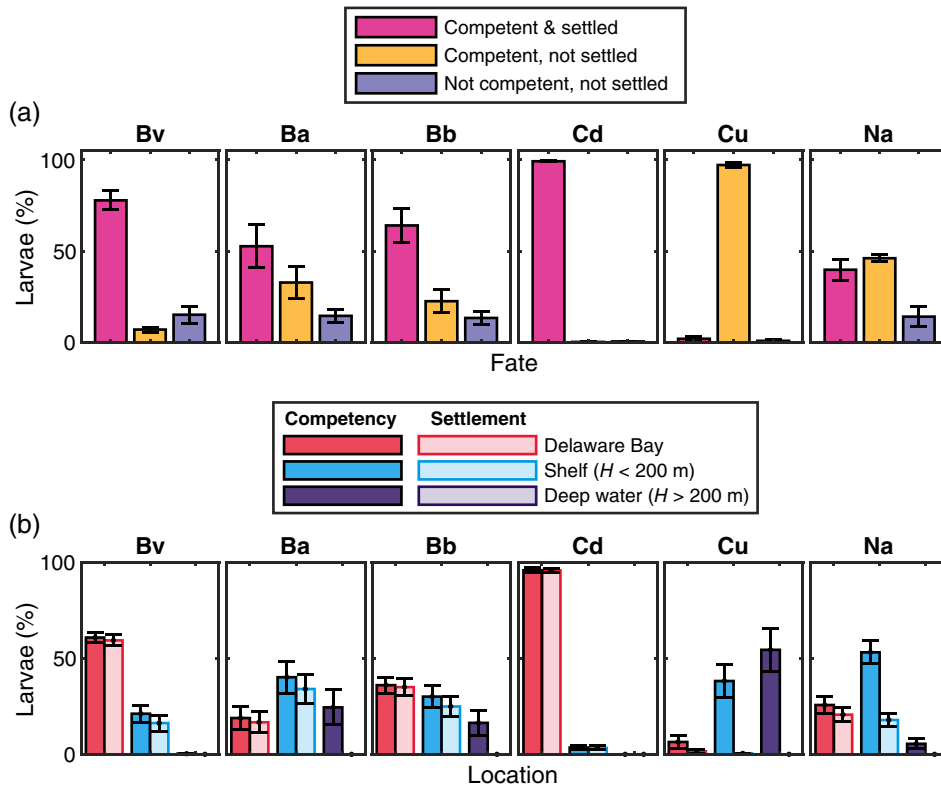


Fig. 3. Larval fate. (a) Percentage of larvae that became competent and settled (pink), became competent but did not settle (yellow), and did not become competent and did not settle (purple). (b) Percentage of larvae that became competent (dark) and settled (light) in Delaware Bay (red), on the shelf (blue), and in waters deeper than 200 m (purple). Abbreviations represent larvae that responded to vorticity only (Bv, inlet mudsnail), to acceleration only (Ba), and to both vorticity and acceleration (Bb, shelf mudsnail), and downward-swimming (Cd), upward-swimming (Cu), and neutrally buoyant (Na) larvae. Percentages are calculated for each year by combining all four release sites ($n = 76,800/\text{year}$). Bars show the average of all annual values, while error bars show the standard error ($n = 6$).

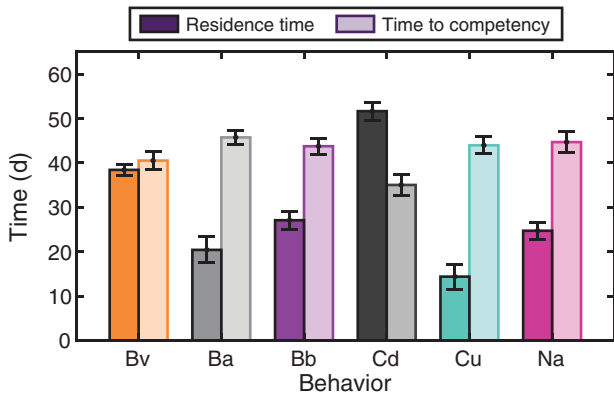


Fig. 4. Average larval residence time in Delaware Bay (dark) and average time to competency (light). Behavior abbreviations are as in Fig. 3. Averages are calculated for each year by combining all four release sites ($n = 76,800/\text{year}$). Bars show the average of all annual values, while error bars show the standard error ($n = 6$).

(Fig. 3b). Neutrally buoyant larvae and larvae that responded only to acceleration primarily became competent on the shelf, while only up-swimming larvae primarily became competent in deep waters (Fig. 3b).

Variations in the location of competency were associated with variations in the timing of competency and transport by local currents, as captured by the average larval residence time (Eq. 2) in Delaware Bay (Fig. 4). Indeed, larvae became competent farther from the bay (distance covered to deep water > shelf > bay) as residence time in the bay decreased (Figs. 3, 4), and most larvae became competent within the bay only when their time to competency was comparable to, or less than, their residence time in the bay (Figs. 3, 4). In general, larvae that spent the most time in Delaware Bay (Fig. 4) became competent more rapidly because estuarine waters were warmer than the adjacent shelf waters (Fig. 1d,e). Despite growing more slowly outside of the estuary, larvae continued to develop and reach competency, implying that larvae expelled onto the shelf could potentially settle in other environments.

Patterns of settlement between Delaware Bay and the continental shelf mirrored those of competency with two exceptions: neutrally buoyant larvae did not settle on the shelf as readily as in the bay, and up-swimming larvae experienced very little settlement (Fig. 3b). As larvae traveled south, settlement reached deeper isobaths, especially for those larvae that responded to acceleration whose settlement reached all depths of the shelf (Supplementary Fig. S2). In contrast, down-swimming larvae and those that responded to vorticity only rarely settled beyond the 20-m and 40-m isobaths, respectively (Supplementary Fig. S2). No settlement occurred beyond the shelfbreak, where larvae never reached the seabed (Fig. 3b & Supplementary Fig. S2).

Settlement in Delaware Bay

Within Delaware Bay, more larvae settled on tidal flats than in the channel for all behaviors tested (Fig. 5a), and larvae that

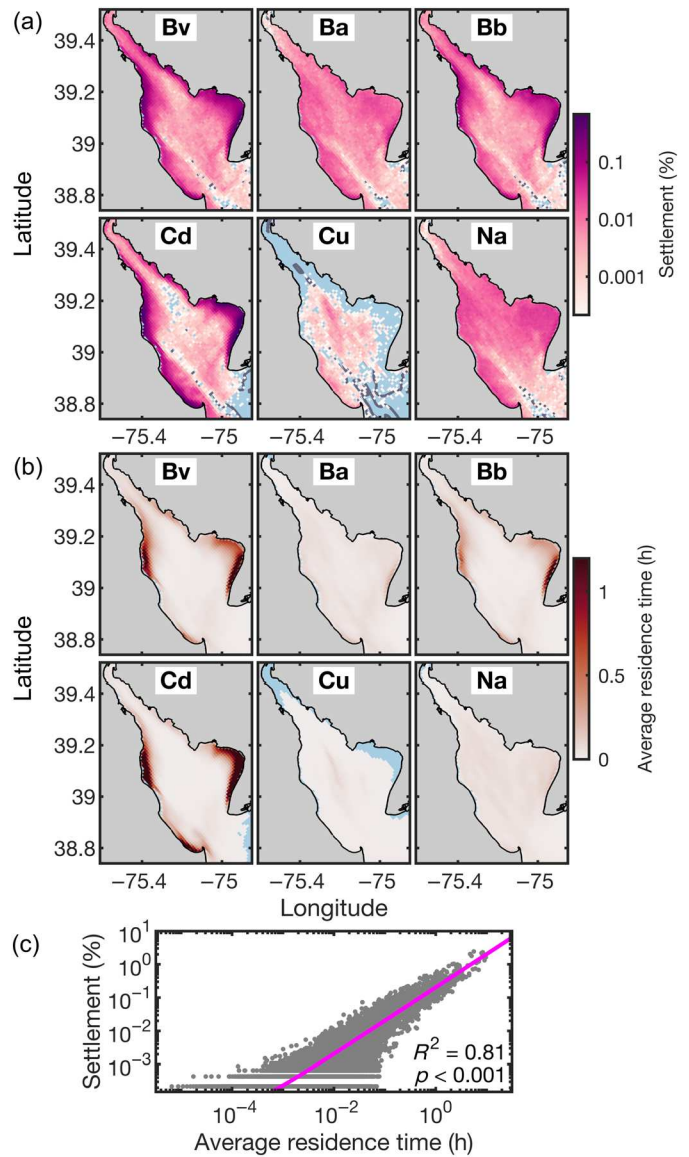


Fig. 5. Maps of (a) settlement (%; $n = 460,800$; \log_{10} scale) and (b) average residence time (Eq. 2) following competency (h). Behavior abbreviations are as in Fig. 3. Cells without larvae are in light blue. (c) Total larval settlement (%) as a function of average residence time while competent (h) for every grid cell in SnailDel. Pink line is a linear fit to untransformed values; slope is statistically significant ($p < 0.001$).

exhibited some downward velocities settled in higher concentrations near the landward edge of the flats (Fig. 5a). Settlement was likely lower in the channel than on the flats due to a combination of higher shear stresses in the channel preventing settlement (Fig. 1f) and increased time spent by competent larvae on the flats (Fig. 5b). Critical shear stresses for competent larvae are on the order of 0.01 Pa. Larvae advected in the channel experienced median bed shear stresses of 0.4 Pa (interquartile range: 0.16–0.73 Pa), compared to 0.29 Pa (interquartile range: 0.1–0.5 Pa) over the flats (red

dots; Fig. 1f). Further, larvae circulating in the middle of the bay were on average younger, smaller, and pre-competent, whereas those circulating at the landward edge of the tidal flats were older, larger, and competent (not shown). Thus, larvae on the flats both were more capable of settling and had more settlement opportunities due to their higher sinking speeds (for larvae whose behavior included passive sinking).

Opportunities for settlement were determined not only by bed shear stresses and time spent in an area, but also by the larvae's vertical positions, which were influenced by larval behavior and size. In the channel and at low shear stresses, pre-competent larvae moving upward—either constantly or in response to acceleration—remained high in the water column, especially near the mouth of the bay where waves and their accelerations were large (Fig. 6a). In contrast, larvae moving downward—either constantly or in response to vorticity—remained low in the water column (Fig. 6a). Larvae that responded to both signals had similar vertical distributions to neutrally buoyant larvae, suggesting that vorticity- or acceleration-induced sinking was counteracted by acceleration-induced upward swimming (Fig. 6a). Following competency, however, sinking speeds are at least twice the speed of

acceleration-induced upward swimming, and both acceleration- and vorticity-induced sinking dominated the vertical movements of responsive larvae, resulting in larvae being concentrated near the seabed for all behaviors except up-swimming and neutrally buoyant larvae (Fig. 6a). The increased near-bed concentrations enhanced settlement opportunities for larvae still in Delaware Bay after competency. At high shear stresses, larvae were mostly mixed throughout the water column (Fig. 6b). Trends in larval vertical distributions on the flats mirrored those in the channel, although vertical separation between behaviors was not as strong (Fig. 6c,d), probably due to stronger mixing and weaker wave accelerations on the flats compared to the channel.

Tidal mixing vs. larval behavior

To better understand the mechanisms controlling larval vertical distributions, we also considered the effects of vertical mixing using simple tidal models and a subset of behaviors unaffected by waves (constant swimming, gyrotactic sinking, and passive sinking). In the more turbulent ebb and flood phases of the tide, that is, when bed shear stress and eddy diffusivity were high, larvae were more evenly distributed and the Péclet number was lower than at low bed shear stresses for constantly swimming or passively sinking larvae (Fig. 7b,d, left). Although the downward velocities of gyrotactic sinkers increased with turbulence, leading to an increase in $Pé$, this behavior was still insufficient to overcome turbulent mixing ($Pé < 1$; Fig. 7c, left). Throughout the boundary layer, the average speeds of gyrotactic sinkers were typically at least 10 times less than the constant swimming speed (-0.05 cm s^{-1}), which was also 10 times less than the passive sinking speed of competent larvae (-0.5 cm s^{-1} ; Fig. 7c, left). Thus, larval Péclet numbers increased from gyrotactic sinkers to constant swimmers to passively sinking larvae (Fig. 7b–d, left), indicating a progressively stronger ability of behavior to concentrate larvae at the seabed in the presence of vertical mixing.

Throughout most of the tidal boundary layer, turbulence-induced sinking was the only reliable means of overcoming mixing for larvae that responded to vorticity ($Pé > 1$; Fig. 7d, left). In the channel, constant swimmers could also become concentrated at a boundary ($Pé > 1$), but their ability to overcome mixing was stronger near the top of the boundary layer than the bottom (Fig. 7b, left). This asymmetry in the ability of larvae to overcome mixing was reflected in the regional model by the higher concentrations of up-swimming larvae near the surface than of down-swimming larvae at the bottom (Fig. 6a). On the flats, the $Pé$ profiles were consistent with the distribution of up- and down-swimming larvae in the regional model, which mirrored each other (Fig. 6c).

Comparing the magnitude of larval and turbulent vertical velocities also highlighted some features of larval distributions not captured by $Pé$ profiles. Focusing on larval distributions in the regional model, we note that distributions in the channel when mixing was strong resembled distributions on the flats when mixing was strong more closely than they resembled

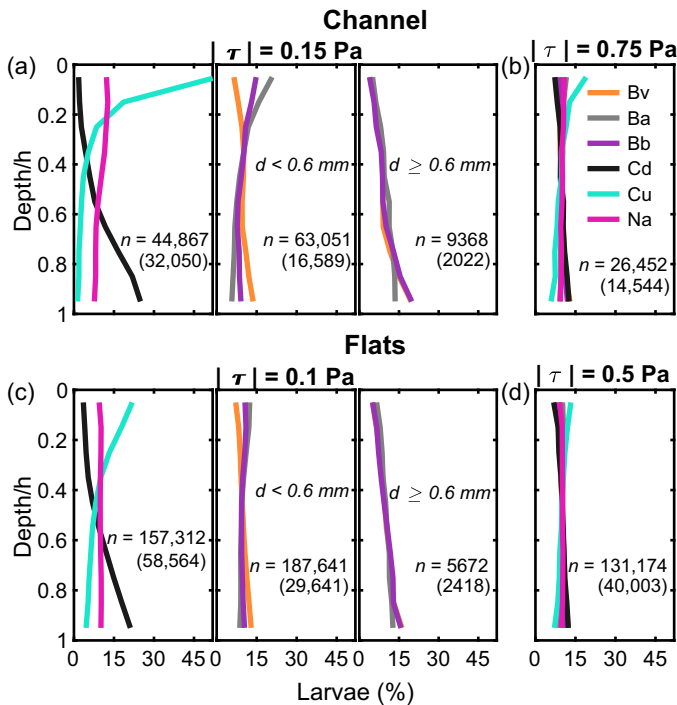


Fig. 6. Larval depths, normalized by the water column height h , (a, b) in the channel and (c, d) on the flats (red dots; Fig. 1f). Behavior abbreviations are as in Fig. 3. Larval depths are shown for low and high shear stresses, indicating tidal phases with weak and strong mixing, respectively. At low shear stresses (a, c) pre-competent ($d < 0.6 \text{ mm}$; middle) and competent ($d \geq 0.6 \text{ mm}$; right) larvae are separated for vorticity- or acceleration-induced behaviors that include passive sinking, which increases with size. Plots include the average number of larvae sampled per behavior (n), with the standard deviation in parentheses.

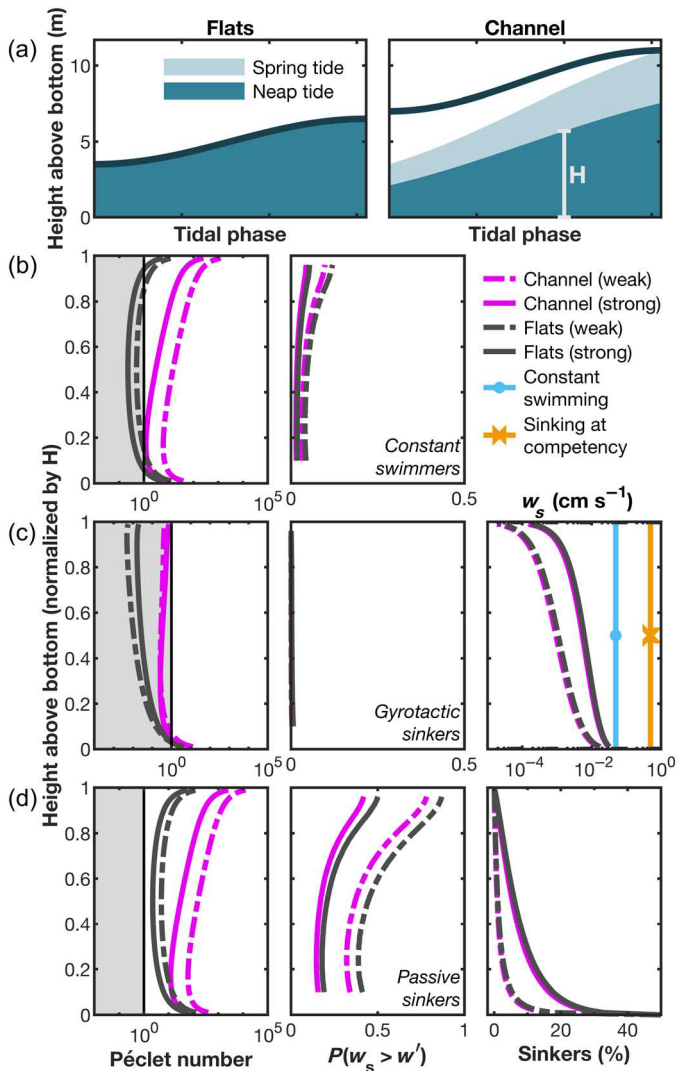


Fig. 7. Tidal model predictions of larval vertical movement. **(a)** Schematics showing the height of the bottom boundary layer H (m), as a function of tidal phase on the flats (left), and in the channel (right). Light and dark colors show spring and neap tides, respectively, while the solid line shows the water column height (m). Note that on the flats, H always spans the water column in both spring and neap tides. **(b)** Larval Péclet number (Eq. 3; left) and probability that the magnitude of larval vertical velocities exceeds that of turbulent vertical velocities (right) for constant swimmers in the channel (pink) and on the flats (dark gray), at low (dashed) and high (solid) bottom shear stresses. $Pé < 1$ (shaded area) indicates that the vertical position of larvae is generally controlled by turbulent mixing, and not by swimming. **(c)** Same as in **(b)** for larvae that respond to vorticity and are swimming and sinking gyrotactically. Average larval swimming speeds (cm s^{-1}) are also shown (right), including constant swimming speed and sinking speed at competency ($d = 600 \mu\text{m}$). **(d)** Same as in **(b)** for larvae that respond to vorticity and are sinking passively. The percentage of larvae sinking passively is also shown (right).

distributions in the channel when mixing was weak (Fig. 6). In other words, larval vertical distributions were primarily governed not by their location in the bay but by the mixing regime. This feature was reproduced by profiles showing the likelihood that

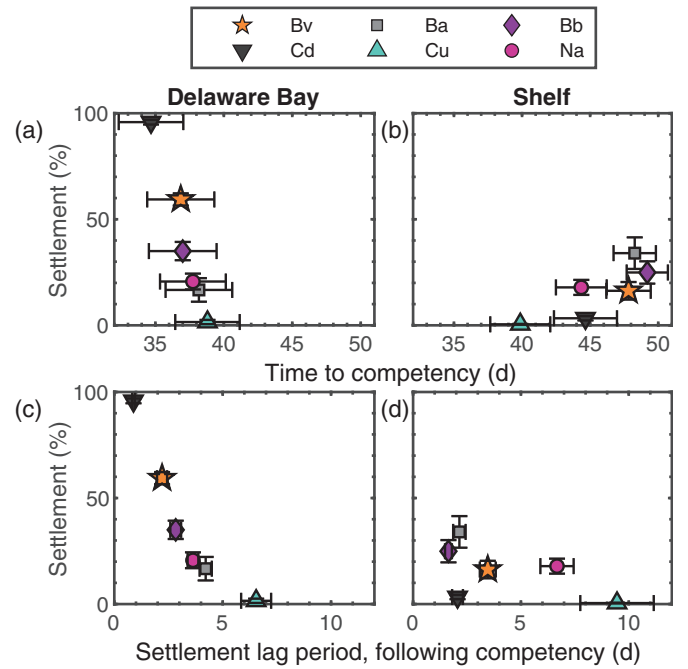


Fig. 8. Percentage of larvae that settled **(a,c)** in Delaware Bay and **(b,d)** on the shelf vs. their **(a,b)** age at competency and **(c,d)** settlement lag period, following competency. Note that $\text{PLD} = \text{age at competency} + \text{settlement lag period}$ (Supplementary Fig. S3). Behavior abbreviations are as in Fig. 3. Percent settled, mean age at settlement, and mean time to settlement are calculated for each year by combining all four release sites ($n = 76,800/\text{year}$). Error bars show the standard errors of these annual values ($n = 6$).

larval velocities exceeded turbulent velocities in magnitude (e.g., Fig. 7, middle column—same-style lines closer together than same-color lines) but not by $Pé$ profiles (e.g., Fig. 7, right—same-color lines closer together than same-style lines), in part because the Péclet number depends on the water column height.

Larval fate

Taking a step back from complex estuarine morphology and circulation, we summarized the costs and benefits of different behaviors using simple ecological metrics: the percentage of larvae that ultimately settled and the time it took to do so (Fig. 8). The time to settlement varied with the time to reach competency and a subsequent lag period affected by larval depth and likelihood of reaching the seabed while tidal velocities were low. There was a clear gradient in overall fitness metrics for larvae settling in Delaware Bay (Fig. 8). Larvae with behaviors involving more frequent downward movement (constant down-swimming > response to vorticity > response to vorticity and acceleration) grew to competency and settled faster, leading to higher settlement percentages, whereas larvae with behaviors involving more frequent up-swimming (constant up-swimming > response to acceleration > response to vorticity and acceleration) grew to competency and settled more slowly, yielding lower settlement percentages in the bay.

Any propensity to sink contributed to increased retention in the bay and particularly over the flats (Fig. 5). High retention over these shallow areas gave larvae more settlement opportunities while also counterintuitively enabling them to grow faster (Fig. 8). Trends were less clear for larvae settling on the shelf, partly due to the large differences in the percentage of larvae exported. Generally, larvae that settled on the shelf grew more slowly than larvae that settled in Delaware Bay. Despite reaching competency the slowest, however, larvae with responses to acceleration had the highest settlement percentages on the shelf and the shortest settlement lag period (Fig. 8), presumably because wave accelerations are large on the shelf, and acceleration-induced sinking speeds exceeded acceleration-induced up-swimming speeds when larvae were of a competent size.

Discussion

Ecological implications of observed behaviors

Our simulations showed that behaviors involving descents were the most conducive to settlement in Delaware Bay because they led to higher concentrations of larvae near the bed, resulting in higher retention and faster growth. The shorter pelagic larval durations (Supplementary Fig. S3) associated with these behaviors could further benefit larvae by reducing overall exposure to predation in the plankton, improving their chances of survival. Although our simulations did not include larval mortality, we estimated its effect (Supplementary Table S3). Assuming a common mortality rate of 0.1 d^{-1} (White et al. 2014a), the adjusted settlement percentage of shelf snail larvae (response to vorticity and acceleration) is an additional 10%–15% lower than that of inlet snail larvae (response to vorticity) and down-swimming larvae.

Although constant downward swimming was the most beneficial behavior based on metrics captured by our simulations (Fig. 8), the model omitted other processes that impact overall fitness such as predation and energetics. Downward swimming concentrated larvae nearest the bottom and would expose them to greater risk from benthic predators (e.g., Morgan 1992), potentially offsetting the benefits of high settlement probabilities. Behaviors can greatly impact fitness via larval energetics, which depends on a complex balance of swimming effort and ability to collect food particles. Compared to downward swimming and passive sinking, hovering carries the highest metabolic cost but also confers the highest feeding efficiency and may be necessary for larval growth (Gallager 1993; Kiørboe and Jiang 2013). In contrast, passive sinking carries no energetic costs but precludes feeding. Yet passive sinking is the fastest means of descent for mollusk larvae and therefore the most efficient behavior for concentrating at the seabed, which is key to retention in strong currents. The observed response to vorticity—hovering in calm conditions and sinking intermittently in turbulence—would enable inlet snails to prioritize energetic gains when currents and turbulence are weak, but

prioritize local retention when currents and turbulence are strong and hovering/feeding becomes more difficult. This ability to optimize both energetics and settlement makes the vorticity response well suited for optimizing overall fitness of estuarine larvae.

In general, we found that the observed acceleration response of shelf mudsnail larvae would be detrimental to inlet mudsnails. The vorticity response of inlet snail larvae was nearly twice as suitable for retention and settlement in estuaries as the combined response to vorticity and acceleration of shelf snail larvae (Fig. 8). Further, competent inlet snail larvae spent more time, and settled more readily, at the landward edge of the bay's tidal flats (Fig. 5), where adult populations of the inlet snail are abundant. Inlet snail larvae also reached Delaware Bay from a wider area along the coast than snail larvae that responded to acceleration, thereby promoting connectivity between bays (Supplementary Fig. S4). In the lab, inlet snail larvae responded weakly to acceleration signals in early stages but lost this response at competency (Fuchs et al. 2018). The taxonomic relationship between the inlet and shelf species is unresolved (Yang et al. 2021), but given that the inlet larvae's acceleration response disappears ontogenetically, we speculate that both species originated on the shelf. Inlet snails may have diverged from their congeneric counterpart as larvae developed an ability to ignore accelerations and were more easily transported into and retained in coastal embayments. The evolution of larval behavior is beyond the scope of our study, but the processes linking behavioral evolution and phylogeny present intriguing areas for future research.

By necessity, our simulations omitted many types of larval behaviors, including ontogenetic migrations and different types of sensitivity to fluid motions. However, our model captured an important ontogenetic change observed in inlet snail larvae; larvae responded similarly to turbulence both before and after competency, but their passive sinking speeds increased ontogenetically as larvae grew (Fuchs et al. 2018). Our generic, constant-swimming behaviors did not include ontogenetic changes (Metaxas and Saunders 2009), which potentially could enable a larger percentage of up-swimming larvae to settle throughout both Delaware Bay and the Mid-Atlantic Bight (Fig. 8 and Supplementary Fig. S2). Our simulations also omitted the turbulence-induced acceleration of competency that has been observed in many echinoderm species (Gaylord et al. 2013; Hodin et al. 2015). This effect could impact the timing and location of settlement but was beyond the scope of our study. We hope that new behavior modules will be developed for ROMSPATH to investigate the dispersal and settlement associated with a range of species-specific empirical behaviors.

Larval depth and estuarine circulation

Within Delaware Bay, larval residence time was primarily controlled by larval depth. As expected, time-averaged bottom

currents in the channel transported near-bed larvae into the bay, while time-averaged surface currents in the channel expelled near-surface larvae onto the shelf. The interaction between lateral currents, tidal mixing, and larval depth was more complex. Lateral circulation in estuaries varies with depth and is typically toward the flats near the bottom and toward the channel near the surface (Lerczak and Geyer 2004; their Fig. 1). In Delaware Bay, lateral currents are strongest at slack tide (Aristizábal and Chant 2014), coinciding with the time when descending larvae are most concentrated near the bottom (and up-swimming larvae at the surface; Fig. 6). This temporal overlap enables descending larvae to be transported preferentially landward, contributing to long residence times over the tidal flats, and vice versa for up-swimming larvae (Fig. 5). To experience preferential landward flow, sinking speeds must be high enough to allow larvae to concentrate near the bed at slack tide but also low enough that larvae remain in suspension (McSweeney 2017). Passively sinking larvae could strike an optimal balance; estimates of transit times throughout the boundary layer (Ross 2006) suggest that passively sinking larvae could reach the bed in tens of minutes, while constant-swimming and gyrotactic-sinking larvae could take a few hours and over a day to do so, respectively. In our regional model, vorticity-induced passive sinking enabled the inlet mudsnail larvae to concentrate near the bottom within a tidal cycle. This result is consistent with observed larval vertical distributions of this species in a tidal inlet (Fuchs et al. 2010).

A strong predictor of settlement success was the new estimate of average larval residence time (Eq. 2; Fig. 5c), which more effectively captured the complexity of larval transport pathways than bulk residence time estimates, such as the total exchange flow (TEF; Lemagie and Lerczak 2015). Over the 6 years simulated, residence times calculated from TEF at the mouth averaged to 28.8 ± 1.9 (standard error) days. Although this time estimate was close to the average residence time of neutrally buoyant larvae, it was twice that of constant up-swimmers and one-third that of constant down-swimmers (Fig. 4). These inconsistencies highlight the fact that residence time estimates derived from particle tracks are more versatile than bulk estimates. TEF does not account for particle behavior, whereas particle-based calculations can be adjusted to answer specific questions (Lemagie and Lerczak 2015; this study), and a single formulation can yield unique, spatially resolved estimates for various behaviors (this study).

Data availability statement

The data-assimilative regional reanalysis we used to nudge the Doppio domain is publicly available online (Wilkin and Levin 2021). The source code and configuration files specific to our simulations have been archived online: SWAN (Gerbi et al. 2022a), ROMS (Gerbi et al. 2022b), and ROMSPATH (Hunter 2021; Garwood et al. 2022). For the complete particle track output, contact the authors.

References

- Abelson, A., and M. Denny. 1997. Settlement of marine organisms in flow. *Annu. Rev. Ecol. Evol. Syst.* **28**: 317–339.
- Aristizábal, M., and R. Chant. 2014. Mechanisms driving stratification in Delaware Bay estuary. *Ocean Dyn.* **64**: 1615–1629. doi:10.1007/s10236-014-0770-1
- Booij, N., R. C. Ris, and L. H. Holthuijsen. 1999. A third-generation wave model for coastal regions: 1. Model description and validation. *J. Geophys. Res. Ocean.* **104**: 7649–7666. doi:10.1029/98JC02622
- Chant, R. J., W. R. Geyer, R. Houghton, E. Hunter, and J. Lerczak. 2007. Estuarine boundary layer mixing processes: Insights from dye experiments. *J. Phys. Oceanogr.* **37**: 1859–1877. doi:10.1175/JPO3088.1
- Chen, J.-L., D. K. Ralston, W. R. Geyer, C. K. Sommerfield, and R. J. Chant. 2018. Wave generation, dissipation, and disequilibrium in an embayment with complex bathymetry. *J. Geophys. Res. Ocean.* **123**: 7856–7876. doi:10.1029/2018JC014381
- Clay, T. W., and D. Grünbaum. 2010. Morphology-flow interactions lead to stage-selective vertical transport of larval sand dollars in shear flow. *J. Exp. Biol.* **213**: 1281–1292. doi:10.1242/jeb.037200
- Crimaldi, J. P., J. K. Thompson, J. H. Rosman, R. J. Lowe, and J. R. Koseff. 2002. Hydrodynamics of larval settlement: The influence of turbulent stress events at potential recruitment sites. *Limnol. Oceanogr.* **47**: 1137–1151. doi:10.4319/lo.2002.47.4.1137
- Daigle, R. M., and A. Metaxas. 2011. Vertical distribution of marine invertebrate larvae in response to thermal stratification in the laboratory. *J. Exp. Mar. Biol. Ecol.* **409**: 89–98. doi:10.1016/j.jembe.2011.08.008
- DiBacco, C., H. L. Fuchs, J. Pineda, and K. Helfrich. 2011. Swimming behavior and velocities of barnacle cyprids in a downwelling flume. *Mar. Ecol. Prog. Ser.* **433**: 131–148. doi:10.3354/meps09186
- Fuchs, H. L., M. G. Neubert, and L. S. Mullineaux. 2007. Effects of turbulence-mediated larval behavior on larval supply and settlement in tidal currents. *Limnol. Oceanogr.* **52**: 1156–1165. doi:10.4319/lo.2007.52.3.1156
- Fuchs, H. L., A. R. Solow, and L. S. Mullineaux. 2010. Larval responses to turbulence and temperature in a tidal inlet: Habitat selection by dispersing gastropods? *J. Mar. Res.* **68**: 153–188. doi:10.1357/002224010793079013
- Fuchs, H. L., E. J. Hunter, E. L. Schmitt, and R. A. Guazzo. 2013. Active downward propulsion by oyster larvae in turbulence. *J. Exp. Biol.* **216**: 1458–1469. doi:10.1242/jeb.079855
- Fuchs, H. L., A. J. Christman, G. P. Gerbi, E. J. Hunter, and F. J. Diez. 2015a. Directional flow sensing by passively stable larvae. *J. Exp. Biol.* **218**: 2782–2792. doi:10.1242/jeb.125096
- Fuchs, H. L., G. P. Gerbi, E. J. Hunter, A. J. Christman, and F. J. Diez. 2015b. Hydrodynamic sensing and behavior by

- oyster larvae in turbulence and waves. *J. Exp. Biol.* **218**: 1419–1432. doi:[10.1242/jeb.118562](https://doi.org/10.1242/jeb.118562)
- Fuchs, H. L., and G. P. Gerbi. 2016. Seascape-level variation in turbulence- and wave-generated hydrodynamic signals experienced by plankton. *Prog. Oceanogr.* **141**: 109–129. doi:[10.1016/j.pocean.2015.12.010](https://doi.org/10.1016/j.pocean.2015.12.010)
- Fuchs, H. L., G. P. Gerbi, E. J. Hunter, and A. J. Christman. 2018. Waves cue distinct behaviors and differentiate transport of congeneric snail larvae from sheltered versus wavy habitats. *Proc. Natl. Acad. Sci.* **115**: E7532–E7540. doi:[10.1073/pnas.1804558115](https://doi.org/10.1073/pnas.1804558115)
- Fujimura, A. G., A. J. H. M. Reniers, C. B. Paris, A. L. Shanks, J. H. Macmahon, and S. G. Morgan. 2014. Numerical simulations of larval transport into a rip-channeled surf zone. *Limnol. Oceanogr.* **59**: 1434–1447. doi:[10.4319/lo.2014.59.4.1434](https://doi.org/10.4319/lo.2014.59.4.1434)
- Gallager, S. M. 1993. Hydrodynamic disturbances produced by small zooplankton: Case study for the veliger larva of a bivalve mollusc. *J. Plankton Res.* **15**: 1277–1296. doi:[10.1093/plankt/15.11.1277](https://doi.org/10.1093/plankt/15.11.1277)
- Gallager, S., H. Yamazaki, and C. Davis. 2004. Contribution of fine-scale vertical structure and swimming behavior to formation of plankton layers on Georges Bank. *Mar. Ecol. Prog. Ser.* **267**: 27–43. doi:[10.3354/meps267027](https://doi.org/10.3354/meps267027)
- Garwood, J. C., H. L. Fuchs, G. P. Gerbi, E. J. Hunter, R. J. Chant, and J. L. Wilkin. 2022. Estuarine retention of larvae: Contrasting effects of behavioral responses to turbulence and waves (particle release information, output summary, and processing code). Zenodo. doi:[10.5281/zenodo.6094076](https://doi.org/10.5281/zenodo.6094076)
- Gaylord, B., J. Hodin, and M. C. Ferner. 2013. Turbulent shear spurs settlement in larval sea urchins. *Proc. Natl. Acad. Sci. U. S. A.* **110**: 6901–6906. doi:[10.1073/pnas.1220680110](https://doi.org/10.1073/pnas.1220680110)
- Gerbi, G. P., S. E. Kastner, and G. Brett. 2015. The role of whittcapping in thickening the ocean surface boundary layer. *J. Phys. Oceanogr.* **45**: 2006–2024. doi:[10.1175/JPO-D-14-0234.1](https://doi.org/10.1175/JPO-D-14-0234.1)
- Gerbi, G. P., E. Hunter, J. L. Wilkin, R. Chant, H. L. Fuchs, and J. C. Garwood. 2022a. SWAN configuration of a nested model of the Mid-Atlantic Bight and Delaware Bay. Zenodo. doi:[10.5281/zenodo.6081147](https://doi.org/10.5281/zenodo.6081147)
- Gerbi, G. P., E. Hunter, J. L. Wilkin, R. Chant, H. L. Fuchs, and J. C. Garwood. 2022b. ROMS configuration of a two-way nested model of the Mid-Atlantic Bight and Delaware Bay. Zenodo. doi:[10.5281/zenodo.6090300](https://doi.org/10.5281/zenodo.6090300)
- Geyer, W. R., and P. MacCready. 2014. The estuarine circulation. *Annu. Rev. Fluid Mech.* **46**: 175–197. doi:[10.1146/annurev-fluid-010313-141302](https://doi.org/10.1146/annurev-fluid-010313-141302)
- Hinze, J. O. 1975. *Turbulence*. McGraw-Hill.
- Hodin, J., M. C. Ferner, G. Ng, C. J. Lowe, and B. Gaylord. 2015. Rethinking competence in marine life cycles: Ontogenetic changes in the settlement response of sand dollar larvae exposed to turbulence. *R. Soc. Open Sci.* **2**: 150114. doi:[10.1098/rsos.150114](https://doi.org/10.1098/rsos.150114)
- Hodin, J., M. C. Ferner, and B. Gaylord. 2020. Choosing the right home: Settlement responses by larvae of six sea urchin species align with hydrodynamic traits of their contrasting adult habitats. *Zool. J. Linn. Soc.* **190**: 737–756. doi:[10.1093/zoolinnean/zlz149](https://doi.org/10.1093/zoolinnean/zlz149)
- Hunter, E. J. 2021. imcslatte/ROMSPath: ROMSPath second release (v1.0.1). Zenodo. doi:[10.5281/zenodo.5597732](https://doi.org/10.5281/zenodo.5597732)
- Hunter, E. J., H. L. Fuchs, J. L. Wilkin, G. P. Gerbi, R. J. Chant, and J. C. Garwood. 2021. ROMSPath v1.0: Offline particle tracking for the regional ocean modeling system (ROMS). *Geosci. Model Dev. Discuss.* [preprint]. doi:[10.5194/gmd-2021-400](https://doi.org/10.5194/gmd-2021-400). In review.
- Jay, D. A., and J. D. Musiak. 1994. Particle trapping in estuarine tidal flows. *J. Geophys. Res.* **99**: 20445–20461. doi:[10.1029/94jc00971](https://doi.org/10.1029/94jc00971)
- Kjørboe, T., and H. Jiang. 2013. To eat and not be eaten: Optimal foraging behaviour in suspension feeding copepods. *J. R. Soc. Interface* **10**: 20120693. doi:[10.1098/rsif.2012.0693](https://doi.org/10.1098/rsif.2012.0693)
- Lemagie, E. P., and J. A. Lerczak. 2015. A comparison of bulk estuarine turnover timescales to particle tracking timescales using a model of the Yaquina Bay estuary. *Estuar. Coasts* **38**: 1797–1814. doi:[10.1007/s12237-014-9915-1](https://doi.org/10.1007/s12237-014-9915-1)
- Lentz, S. J., and M. R. Fewings. 2012. The wind- and wave-driven inner-shelf circulation. *Ann. Rev. Mar. Sci.* **4**: 317–343. doi:[10.1146/annurev-marine-120709-142745](https://doi.org/10.1146/annurev-marine-120709-142745)
- Lerczak, J. A., and W. R. Geyer. 2004. Modeling the lateral circulation in straight, stratified estuaries. *J. Phys. Oceanogr.* **34**: 1410–1428. doi:[10.1175/1520-0485\(2004\)034<1410:MTLCIS>2.0.CO;2](https://doi.org/10.1175/1520-0485(2004)034<1410:MTLCIS>2.0.CO;2)
- Levin, L. A. 2006. Recent progress in understanding larval dispersal: New directions and digressions. *Integr. Comp. Biol.* **46**: 282–297. doi:[10.1093/icb/ijc024](https://doi.org/10.1093/icb/ijc024)
- Levin, J., J. Wilkin, N. Fleming, and J. Zavala-Garay. 2018. Mean circulation of the Mid-Atlantic Bight from a climatological data assimilative model. *Ocean Model.* **128**: 1–14. doi:[10.1016/j.ocemod.2018.05.003](https://doi.org/10.1016/j.ocemod.2018.05.003)
- Levin, J., H. G. Arango, B. Laughlin, J. Wilkin, and A. M. Moore. 2019. The impact of remote sensing observations on cross-shelf transport estimates from 4D-Var analyses of the Mid-Atlantic Bight. *Adv. Sp. Res.* **68**: 12. doi:[10.1016/j.asr.2019.09.012](https://doi.org/10.1016/j.asr.2019.09.012)
- López, A. G., J. L. Wilkin, and J. C. Levin. 2020. Doppio-a ROMS (v3.6)-based circulation model for the Mid-Atlantic Bight and Gulf of Maine: Configuration and comparison to integrated coastal observing network observations. *Geosci. Model Dev.* **13**: 3709–3729. doi:[10.5194/gmd-13-3709-2020](https://doi.org/10.5194/gmd-13-3709-2020)
- McSweeney, J. 2017. *Sediment transport dynamics in Delaware estuary*. Rutgers University.
- Metaxas, A. 2001. Behaviour in flow: Perspectives on the distribution and dispersion of meroplanktonic larvae in the

- water column. *Can. J. Fish. Aquat. Sci.* **58**: 86–98. doi:10.1139/f00-159
- Metaxas, A., and M. Saunders. 2009. Quantifying the “bio-” components in biophysical models of larval transport in marine benthic invertebrates: Advances and pitfalls. *Biol. Bull.* **216**: 257–272. doi:10.2307/25548159
- Monismith, S. G., and D. A. Fong. 2004. A note on the potential transport of scalars and organisms by surface waves. *Limnol. Oceanogr.* **49**: 1214–1217. doi:10.4319/lo.2004.49.4.1214
- Morgan, S. G. 1992. Predation by planktonic and benthic invertebrates on larvae of estuarine crabs. *J. Exp. Mar. Bio. Ecol.* **163**: 91–110. doi:10.1016/0022-0981(92)90149-5
- Morgan, S. G., A. L. Shanks, J. Macmahon, A. J. H. M. Reniers, C. D. Griesemer, M. Jarvis, and A. G. Fujimura. 2017. Surf zones regulate larval supply and zooplankton subsidies to nearshore communities. *Limnol. Oceanogr.* **62**: 2811–2828. doi:10.1002/lno.10609
- North, E. W., Z. Schlag, R. R. Hood, M. Li, L. Zhong, T. Gross, and V. S. Kennedy. 2008. Vertical swimming behavior influences the dispersal of simulated oyster larvae in a coupled particle-tracking and hydrodynamic model of Chesapeake Bay. *Mar. Ecol. Prog. Ser.* **359**: 99–115. doi:10.3354/meps07317
- Pareja-Roman, L. F., R. J. Chant, and D. K. Ralston. 2019. Effects of locally generated wind waves on the momentum budget and subtidal exchange in a coastal plain estuary. *J. Geophys. Res. Ocean.* **124**: 1005–1028. doi:10.1029/2018JC014585
- Paris, C. B., L. M. Chérubin, and R. K. Cowen. 2007. Surfing, spinning, or diving from reef to reef: Effects on population connectivity. *Mar. Ecol. Prog. Ser.* **347**: 285–300. doi:10.3354/meps06985
- Pechenik, J. A. 1978. Winter reproduction in the gastropod *Nassarius trivittatus*. *Veliger* **21**: 297–298.
- Pineda, J., and N. Reynolds. 2018. Larval transport in the coastal zone: Biological and physical processes, p. 145–163. *In* T. J. Carrier, A. M. Reitzel, and A. Heyland [eds.], *Evolutionary ecology of marine invertebrate larvae*. Oxford Univ. Press.
- Pringle, J. M., and P. J. S. Franks. 2001. Asymmetric mixing transport: A horizontal transport mechanism for sinking plankton and sediment in tidal flows. *Limnol. Oceanogr.* **46**: 381–391. doi:10.4319/lo.2001.46.2.0381
- Ris, R. C., L. H. Holthuijsen, and N. Booij. 1999. A third-generation wave model for coastal regions: 2. Verification. *J. Geophys. Res. Ocean.* **104**: 7667–7681. doi:10.1029/1998JC900123
- Ross, O. N., and J. Sharples. 2004. Recipe for 1-D Lagrangian particle tracking models in space-varying diffusivity. *Limnol. Oceanogr. Methods* **2**: 289–302. doi:10.4319/lom.2004.2.289
- Ross, O. N. 2006. Particles in motion: How turbulence affects plankton sedimentation from an oceanic mixed layer. *Geophys. Res. Lett.* **33**: 1–5. doi:10.1029/2006GL026352
- Roy, A., A. Metaxas, and T. Ross. 2012. Swimming patterns of larval *Strongylocentrotus droebachiensis* in turbulence in the laboratory. *Mar. Ecol. Prog. Ser.* **453**: 117–127. doi:10.3354/meps09662
- Scheltema, R. S. 1961. Metamorphosis of the veliger larvae of *Nassarius obsoletus* (Gastropoda) in response to bottom sediment. *Biol. Bull.* **120**: 92–109. doi:10.2307/1539340
- Scheltema, R. S. 1965. The relationship of salinity to larval survival and development in *Nassarius obsoletus* (Gastropoda). *Biol. Bull.* **129**: 340–354. doi:10.2307/1539850
- Scheltema, R. S. 1967. The relationship of temperature to the larval development of *Nassarius obsoletus* (Gastropoda). *Biol. Bull.* **132**: 253–265. doi:10.2307/1539893
- Shchepetkin, A. F., and J. C. McWilliams. 2005. The regional oceanic modeling system (ROMS): A split-explicit, free-surface, topography-following-coordinate oceanic model. *Ocean Model.* **9**: 347–404. doi:10.1016/j.ocemod.2004.08.002
- Simons, R. D., D. A. Siegel, and K. S. Brown. 2013. Model sensitivity and robustness in the estimation of larval transport: A study of particle tracking parameters. *J. Mar. Syst.* **119–120**: 19–29. doi:10.1016/j.jmarsys.2013.03.004
- Simpson, J. H., J. Brown, J. Matthews, and G. Allen. 1990. Tidal straining, density currents, and stirring in the control of estuarine stratification. *Estuaries* **13**: 125–132. doi:10.2307/1351581
- Soulsby, R. L., and R. J. S. Whitehouse. 1997. Threshold of sediment motion in coastal environments. *Proceedings Pacific Coasts and Ports 1997 Conference*. Centre for Advanced Engineering, University of Canterbury. 149–154.
- Thomson, J., M. S. Schwendeman, S. F. Zippel, S. Moghimi, J. Gemmrich, and W. E. Rogers. 2016. Wave-breaking turbulence in the ocean surface layer. *J. Phys. Oceanogr.* **46**: 1857–1870. doi:10.1175/JPO-D-15-0130.1
- Trowbridge, J. H. 1992. A simple description of the deepening and structure of a stably stratified flow driven by a surface stress. *J. Geophys. Res.* **97**: 15529–15543. doi:10.1029/92jc01512
- Umlauf, L., and H. Burchard. 2003. A generic length-scale equation for geophysical turbulence models. *J. Mar. Res.* **61**: 235–265. doi:10.1357/002224003322005087
- Welch, J. M., and R. B. Forward. 2001. Flood tide transport of blue crab, *Callinectes sapidus*, postlarvae: Behavioral responses to salinity and turbulence. *Mar. Biol.* **139**: 911–918. doi:10.1007/s002270100649
- Wheeler, J. D., K. R. Helfrich, E. J. Anderson, and L. S. Mullineaux. 2015. Isolating the hydrodynamic triggers of the dive response in eastern oyster larvae. *Limnol. Oceanogr.* **60**: 1332–1343. doi:10.1002/lno.10098
- White, J. W., S. G. Morgan, and J. L. Fisher. 2014a. Planktonic larval mortality rates are lower than widely expected. *Ecology* **95**: 3344–3353. doi:10.1890/13-2248.1
- White, J. W., A. Rassweiler, J. F. Samhoury, A. C. Stier, and C. White. 2014b. Ecologists should not use statistical

- significance tests to interpret simulation model results. *Oikos* **123**: 385–388. doi:[10.1111/j.1600-0706.2013.01073.x](https://doi.org/10.1111/j.1600-0706.2013.01073.x)
- Wilkin, J., J. Levin, A. Lopez, E. Hunter, J. Zavala-Garay, and H. Arango. 2018. A Coastal Ocean forecast system for U.S. mid-Atlantic bight and gulf of Maine, p. 593–624. *In* E. Chassignet, A. Pascual, J. Tintoré, and J. Verron [eds.], *New Frontiers in operational oceanography*. GODAE OceanView.
- Wilkin, J., and J. Levin. 2021. Outputs from a Regional Ocean modeling system (ROMS) data assimilative reanalysis (version DopAnV2R3-ini2007) of ocean circulation in the mid-Atlantic bight and gulf of Maine for 2007-2020. SEANOE. doi:[10.17882/86286](https://doi.org/10.17882/86286)
- Yang, Y., S. Abalde, C. L. M. Afonso, M. J. Tenorio, N. Puillandre, J. Templado, and R. Zardoya. 2021. Mitogenomic phylogeny of mud snails of the mostly Atlantic/Mediterranean genus *Tritia* (Gastropoda: Nassariidae). *Zool. Scr.* **50**: zsc.12489. doi:[10.1111/zsc.12489](https://doi.org/10.1111/zsc.12489)

Acknowledgments

The authors thank Associate Editor James Leichter and three anonymous reviewers for encouraging feedback that significantly improved the manuscript. The authors are also grateful to Julia Levin and Alex López for help with model development and Doppio, Samantha Kenah, Claire Mundi and Jeremy Wilson for early work on particle tracking output, Elizabeth North and Zachary Schlag for making LTRANS v.2, upon which ROMSPath is built, freely available, and Rutgers University Libraries for covering the Open Access charges. This material is based upon work supported by the National Science Foundation under Grants OCE-1756646 to HLF and RJC, and OCE-1756591 and OCE-2051795 to GPG. Code to recreate the analyses and figures in this manuscript is available at <https://zenodo.org/record/6094076>.

Conflict of interest

None declared.

Submitted 08 August 2021

Revised 12 January 2022

Accepted 09 February 2022

Associate editor: James J. Leichter

Supplementary information

Supplemental Methods

S1. Model forcing

Open boundary values for the outer-domain model were set from Mercator-Océan daily averages (Lellouche et al. 2018). Meteorological forcing over the entire model domain used the North American Regional Reanalysis (NARR; Mesinger et al. 2006) and the North American Mesoscale forecast model (NAM; Janjic et al. 2005) with air-sea fluxes computed via bulk formulae (Fairall et al. 2003). River runoff was prescribed using United States Geological Survey (USGS) and Water Survey of Canada (WSC) data following the method of López et al. (2020). To prevent drift of bottom water conditions toward unrealistic values, temperature and salinity in the Doppio domain were nudged with a three-day timescale to a data-assimilative regional reanalysis (Wilkin et al. 2018; Wilkin and Levin 2021).

Wave conditions were computed with SWAN (Booij et al. 1999; Ris et al. 1999) on the same model grids as ROMS and with the same meteorological forcing. Wave open boundary conditions for the Doppio domain were drawn from NOAA Wavewatch III (Tolman 2002), and the Doppio SWAN solution provided boundary values to the SnailDel wave simulation. The two wave grids were otherwise uncoupled. ROMS and SWAN model configuration files for our simulations are available online (Gerbi et al. 2022a, 2022b).

S2. ROMSPath

ROMSPath is an offline particle tracking software based on LTRANS (North et al. 2008) that includes improvements and newly added features necessary for this study (Hunter 2021; Hunter et al. 2021). Particle trajectories are computed in ROMS native coordinates to obviate unnecessary interpolations and improve accuracy and efficiency; tracking across the nested grids interface is supported; Stokes drift is added to larval advection; and advective and diffusive time steps are distinct (Hunter 2021; Hunter et al. 2021). The immediate larval environment was assessed every minute by linearly interpolating hydrodynamic model output to larval positions. Larvae were advected in the model domain using Stokes velocities calculated from the wave model output (SWAN) added linearly to ROMS velocities and velocities due to behavior (see *Behavior models and Supplemental Methods S4*). Vertical turbulent motions were incorporated using a random walk model with 1-s time steps (J. R. Hunter et al., 1993; Visser 1997; E. J. Hunter et al. 2021). Larval 3-D positions, sizes, and the fluid characteristics they encountered (temperature, bottom shear stress, vorticity, acceleration) were saved hourly for each virtual larva.

S3. Behavior signals

Turbulence-generated signals are intermittent, and their probability density functions (PDFs) are symmetric with long flat tails, that is, with high kurtosis K . Isotropic turbulence has statistical properties invariant to rotation, and the variances of each horizontal (x and y) component of vorticity ($\sigma_{\zeta x}^2$ and $\sigma_{\zeta y}^2$) and acceleration ($\sigma_{a'x}^2$ and $\sigma_{a'y}^2$) were computed as

$$\sigma_{\zeta x}^2 = \sigma_{\zeta y}^2 = \frac{\epsilon}{3\nu}, \text{ and} \tag{S1}$$

$$\sigma_{\alpha'x}^2 = \sigma_{\alpha'y}^2 = \frac{a_0 \epsilon^{3/2}}{\nu^{1/2}}, \quad (\text{S2})$$

where ϵ is the dissipation rate of turbulent kinetic energy, ν is the kinematic viscosity, and a_0 is a constant between 1 and 10; we use $a_0 = 5$ (Taylor 2002; Voth et al. 2002). At high Reynolds number, the PDFs generally have $K = 10$ to 30 for vorticity (Van Atta and Antonia 1980), and $K = 20$ to 50 for acceleration (Voth et al. 2002). In practice, it is difficult to generate random number distributions that have K as high as that of turbulence-induced signals ($K > 10$; Van Atta and Antonia 1980; Voth et al. 2002) because large values in the tails have extremely low probabilities. Instead, we used a Laplace distribution ($K = 6$), which adequately captured the frequency of high-magnitude turbulence events within the modeled larval life span.

Wave-generated accelerations are normally distributed, and acceleration in each horizontal direction is determined by the details of the wave field. The variances of the horizontal components of acceleration were computed as

$$\sigma_{\tilde{\alpha}}^2 = \int_0^{2\pi} \int_0^\infty \frac{\omega^4 \cosh^2(k(z+h))}{\sinh^2(kh)} S(\omega, \theta) \text{fn}(\theta) d\omega d\theta, \quad (\text{S3})$$

where ω is the wave frequency, k is the wavenumber, h is the water column height, θ is the direction counterclockwise from the x -axis, S is the directional sea surface displacement spectrum, $\text{fn}(\theta) = \cos^2(\theta)$ or $\text{fn}(\theta) = \sin^2(\theta)$ for the x - or y -direction, respectively, and $z = 0$ is the undisturbed sea surface (positive up).

S4. Larval behavior

Larval responses to vorticity and acceleration were specified based on previous observations (Fig. 2; Fuchs et al. 2018). At every time step and for the appropriate signal, each larva was identified as sinking or swimming (Fig. 2A), and a velocity for the appropriate behavior was then determined (Fig. 2B-D). The probability of sinking versus swimming and the swimmer's velocity both followed the same functional form of a logistic equation:

$$y = y_0 + \frac{y_s - y_0}{1 + \exp(-4c)}. \quad (\text{S4})$$

Here, y represents either a probability of sinking or a swimming velocity, y_0 is the value of that quantity in still water, and y_s represents the asymptotic maximum (or minimum) value of that quantity in turbulence or waves. The exponential parameter c is a function of the magnitude of either vorticity or acceleration:

$$c = \frac{\ln(x) - \ln(\sqrt{x_c x_s})}{\ln(x_c) - \ln(x_s)}, \quad (\text{S5})$$

where x represents the magnitude of the signal strength (vorticity or acceleration), x_c is a critical minimum value and x_s is a saturation value. At signal strengths smaller than x_c the sinking probability or swimming velocity approach their still-water values, y_0 . At signal strengths larger than x_s the sinking probability or swimming velocity approach their saturation values, y_s . For a single larva, Eq. S4 was used as many as four times at each time step: twice to compute sinking probability and swimming velocity in the presence of vorticity, and again in the presence of

acceleration. For larvae that responded to both signals (shelf snail), the sinking probability was set to the maximum of that computed for vorticity and acceleration, assuming that the larval impulse to retract its velum and sink was set by the stronger signal. For those larvae that continued to swim, swimming velocities were computed as the sum of the two responses, assuming that larval velocity is affected by vorticity-induced rotation, the mechanism behind gyrotactic sinking, even while larvae swim up with greater effort. The exponential parameter c (Eq. S5) was computed only once for acceleration and once for vorticity.

Specifics of the behavior model were selected based on experimental observations (Fig. 2A, Table S1; Fuchs et al. 2018). For responses to either vorticity or acceleration, the percentage of larvae sinking passively ranged from zero in calm water ($x < x_c$) to 50% at signals above saturation ($x > x_s$; Fig. 2A, Table S1). In calm water, larvae had net vertical swimming velocities $w_{swim} = 0$, implying that they acted as neutrally buoyant particles (Fig. 2C and D, Table S1). For larvae responding to vorticity, larval swimming velocity decreased (became more negative/downward) with vorticity and saturated at $w_{swim} = -0.05 \text{ cm s}^{-1}$ to simulate experimental observations of gyrotactic sinking (Fig. 2C, Table S1). For larvae responding to acceleration, larval swimming velocity increased with acceleration and saturated at $w_{swim} = 0.2 \text{ cm s}^{-1}$ to simulate the experimentally observed increase in swimming effort (Fig. 2D, Table S1). Sinking velocities were computed from larval size and density (1060 kg m^{-3} ; Fuchs et al. 2018) using Rubey's (1933) modification of Stokes' law for spherical particles with particle Reynolds numbers > 1 (Fig. 2B; Fuchs et al. 2013, 2015b).

S5. Tidal boundary layer models

Tidal flats were assumed to be unstratified, and the boundary layer H was depth-limited – that is, it spanned the entire water column depth (Fig. 7A). The vertical structure of diffusivity (Fig. S1A) was calculated as:

$$K_z(z_b) = \kappa u_* \frac{z_b(H-z_b)}{H}, \quad (\text{S6})$$

where $\kappa = 0.4$ is the von Kármán constant, $u_* = \sqrt{\tau/\rho}$ is the shear velocity, and z_b is the height above bottom, with $z_b = 0$ at the seabed and positive up. Note that the z -coordinates differ from those used in the hydrodynamic models and ROMSPATH. Dissipation rate (Fig. S1B) was prescribed by assuming a log-layer velocity profile and stress linearly varying from u_*^2 at $z_b = 0$ to 0 at $z_b = H$ (Stacey and Ralston 2005):

$$\epsilon(z_b) = \frac{u_*^3(H-z_b)}{\kappa H z_b}. \quad (\text{S7})$$

The tidal channel of Delaware Bay is stratified, so Eqs. S6 and S7 were adapted to account for stratification following the method of Chant et al. (2007):

$$K_z(z) = \chi \frac{z_b u_*^2}{HN} \frac{\tanh[\alpha(1-\xi)]}{\alpha \text{sech}^2[\alpha(1-\xi)]}, \text{ and} \quad (\text{S8})$$

$$\epsilon(z_b) = (1 - R_f) \frac{u_*^3(H-z_b)}{\kappa H z_b}, \quad (\text{S9})$$

where χ and α are constants equal to 0.61 and 3, respectively, N is the buoyancy frequency, and R_f is the flux Richardson number, set to 0.1 (Chant et al. 2007). In contrast to the tidal flats, the tidal channel's boundary layer depth H typically is less than the full water column depth (Fig. 7B).

The variance of turbulent vertical velocities σ_{wv} , was estimated by fitting a fourth-order polynomial to observations of boundary layers (Hinze 1975; their Fig. 7-19):

$$\frac{\sigma_{wv}^2}{u_*^2} = 0.61 + 3.49 \left(\frac{z_b}{H}\right) - 9.22 \left(\frac{z_b}{H}\right)^2 + 5.75 \left(\frac{z_b}{H}\right)^3 - 0.52 \left(\frac{z_b}{H}\right)^4, \quad (\text{S10})$$

where $0.09 < \frac{z_b}{H} < 0.96$ (Fig. S1C). Turbulent vertical velocities were then calculated by resampling a normal distribution (with zero mean) one million times, and the probability that larval vertical velocities exceeded turbulent vertical velocities was recorded.

Supplemental Tables

Table S1. Input parameters for the behavior models.

| | Signal thresholds | | Sinking probability | | Swimming velocity | |
|-----------------------|-----------------------|----------------------|---------------------|-------|----------------------|--------------------------|
| | x_c | x_s | y_0 | y_s | y_0 | y_s |
| Vorticity response | 1 s ⁻¹ | 10 s ⁻¹ | 0 | 0.5 | 0 cm s ⁻¹ | -0.05 cm s ⁻¹ |
| Acceleration response | 0.1 m s ⁻² | 10 m s ⁻² | 0 | 0.5 | 0 cm s ⁻¹ | 0.2 cm s ⁻¹ |

Table S2. Start date of temperature-triggered (8°C) releases.

| | 2010 | 2011 | 2012 | 2013 | 2014 | 2015 |
|--------|----------|----------|-------------|---------|---------|---------|
| Site 1 | March 22 | March 20 | March 6 | April 7 | April 5 | April 2 |
| Site 2 | March 25 | March 20 | February 29 | April 6 | April 5 | April 4 |
| Site 3 | March 26 | March 22 | February 27 | April 7 | April 8 | April 7 |
| Site 4 | March 19 | March 16 | March 1 | April 4 | April 3 | April 2 |

Table S3. Adjusted settlement percentage in Delaware Bay, assuming fixed mortality rates of 0.01 and 0.1 d⁻¹ over the average time required for settlement. Abbreviations represent larvae that responded to vorticity only (Bv, inlet mudsnail), to acceleration only (Ba), and to both vorticity and acceleration (Bb, shelf mudsnail), and downward-swimming (Cd), upward-swimming (Cu), and neutrally buoyant (Na) larvae.

| | Bv | Ba | Bb | Cd | Cu | Na |
|---------------------------------------|-----|-----|-----|-----|------|-----|
| No mortality (simulations) | 59 | 17 | 35 | 96 | 1.5 | 21 |
| Low mortality (0.01 d ⁻¹) | 40 | 11 | 23 | 67 | 1.0 | 14 |
| High mortality (0.1 d ⁻¹) | 1.0 | 0.2 | 0.5 | 2.3 | 0.01 | 0.3 |

Supplemental Figures

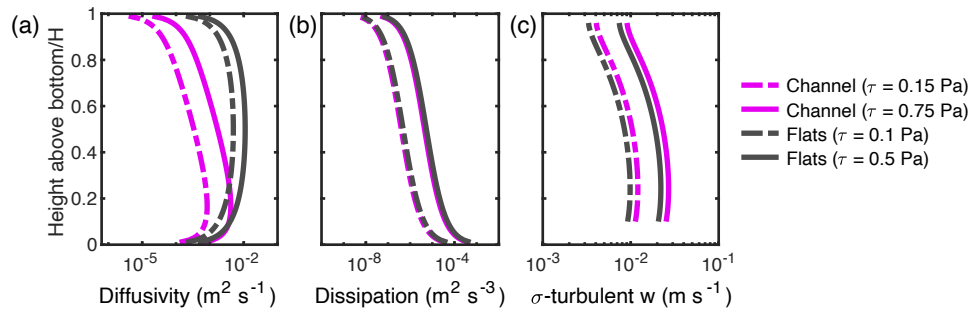


Fig. S1. Tidal models. (a) Predicted bottom boundary layer diffusivity ($\text{m}^2 \text{s}^{-1}$), (b) dissipation rate ($\text{m}^2 \text{s}^{-3}$), and (c) standard deviation of turbulent vertical velocities (m s^{-1}) in the channel (pink) and on the flats (dark gray), at low (dashed) and high (solid) bottom shear stresses.

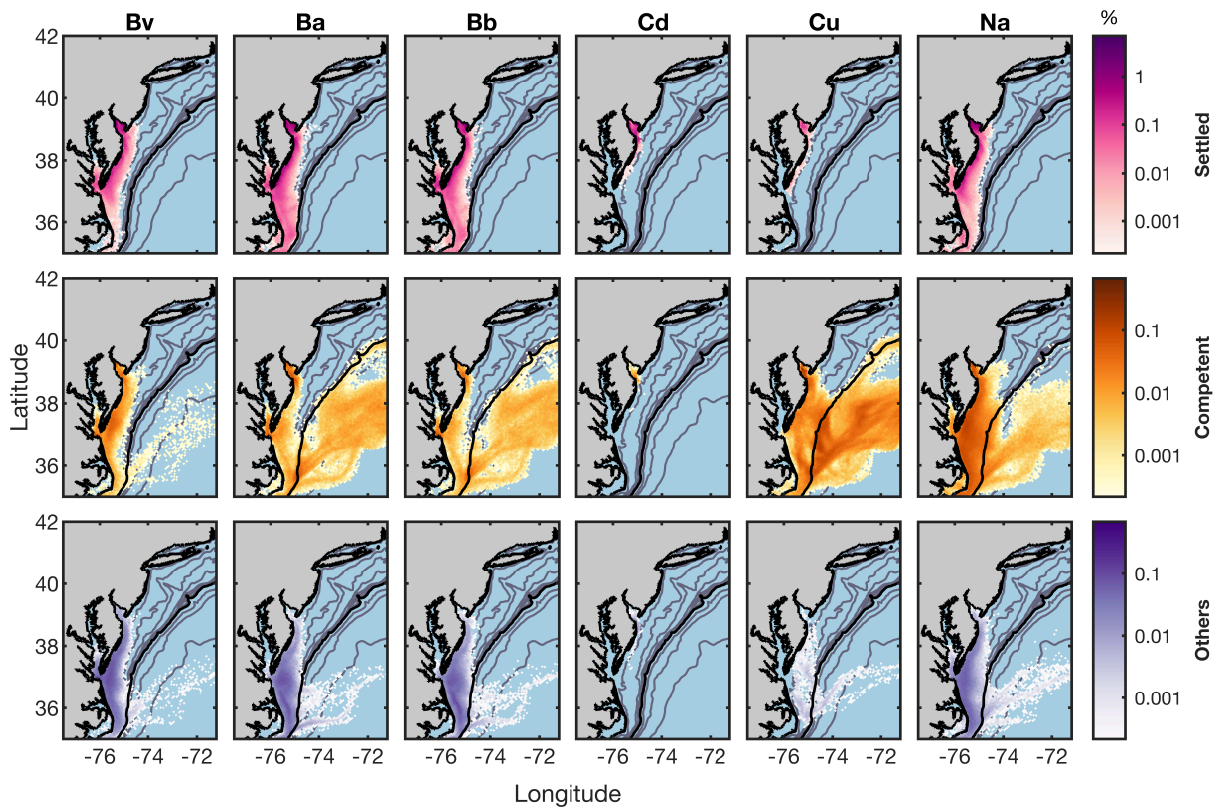


Fig. S2. Location at the end of the pelagic larval duration for larvae that became competent and settled at the first opportunity (top), became competent but had no opportunity for settlement (middle), and did not become competent and did not settle (bottom). Behavior abbreviations are as in Table S3. Colors show the percentage of larvae per grid cell (\log_{10} scale, $n = 460,800$).

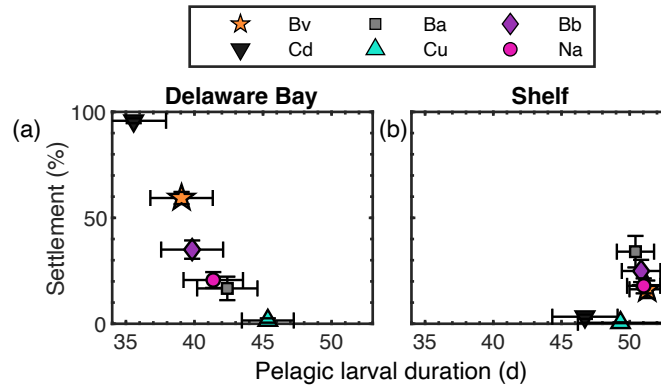


Fig. S3. Percentage of larvae that settled (a) in Delaware Bay and (b) on the shelf versus their pelagic larval duration (d). Behavior abbreviations are as in Table S3.

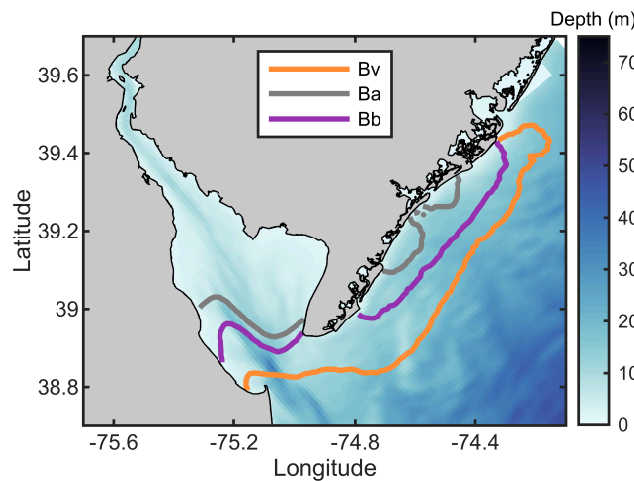


Fig. S4. Contours showing the source locations from which 25% of the larvae were found in Delaware Bay after competency, focusing on larvae with responses to vorticity and acceleration. From separate simulations in which larvae were released throughout the domain from March to June; all years combined.

Supplemental references

- Van Atta, C. W., and R. A. Antonia. 1980. Reynolds number dependence of skewness and flatness factors of turbulent velocity derivatives. *Phys. Fluids* **23**: 252–257.
doi:10.1063/1.862965
- Booij, N., R. C. Ris, and L. H. Holthuijsen. 1999. A third-generation wave model for coastal regions: 1. Model description and validation. *J. Geophys. Res. Ocean.* **104**: 7649–7666.
doi:10.1029/98JC02622
- Chant, R. J., W. R. Geyer, R. Houghton, E. Hunter, and J. Lerczak. 2007. Estuarine boundary layer mixing processes: Insights from dye experiments. *J. Phys. Oceanogr.* **37**: 1859–1877.
doi:10.1175/JPO3088.1
- Fairall, C. W., E. F. Bradley, J. E. Hare, A. A. Grachev, and J. B. Edson. 2003. Bulk parameterization of air–sea fluxes: Updates and verification for the COARE algorithm. *J.*

- Clim. **16**: 571–591. doi:10.1175/1520-0442(2003)016<0571:BPOASF>2.0.CO;2
- Fuchs, H. L., G. P. Gerbi, E. J. Hunter, and A. J. Christman. 2018. Waves cue distinct behaviors and differentiate transport of congeneric snail larvae from sheltered versus wavy habitats. *Proc. Natl. Acad. Sci.* **115**: E7532–E7540. doi:10.1073/pnas.1804558115
- Fuchs, H. L., G. P. Gerbi, E. J. Hunter, A. J. Christman, and F. J. Diez. 2015. Hydrodynamic sensing and behavior by oyster larvae in turbulence and waves. *J. Exp. Biol.* **218**: 1419–1432. doi:10.1242/jeb.118562
- Fuchs, H. L., E. J. Hunter, E. L. Schmitt, and R. A. Guazzo. 2013. Active downward propulsion by oyster larvae in turbulence. *J. Exp. Biol.* **216**: 1458–1469. doi:10.1242/jeb.079855
- Gerbi, G. P., E. Hunter, J. L. Wilkin, R. Chant, H. L. Fuchs, and J. C. Garwood. 2022a. SWAN configuration of a nested model of the Mid-Atlantic Bight and Delaware Bay. Zenodo. doi:10.5281/zenodo.6081147
- Gerbi, G. P., E. Hunter, J. L. Wilkin, R. Chant, H. L. Fuchs, and J. C. Garwood. 2022b. ROMS configuration of a two-way nested model of the Mid-Atlantic Bight and Delaware Bay. Zenodo. doi:10.5281/zenodo.6090300
- Hinze, J. O. 1975. *Turbulence*, McGraw-Hill.
- Hunter, E. J. 2021. imcslatte/ROMSPath: ROMSPath Second Release (v1.0.1). Zenodo. doi:10.5281/zenodo.5597732
- Hunter, E. J., H. L. Fuchs, J. L. Wilkin, G. P. Gerbi, R. J. Chant, and J. C. Garwood. 2021. ROMSPath v1.0: Offline particle tracking for the Regional Ocean Modeling System (ROMS). *Geosci. Model Dev. Discuss.* [preprint]. doi:10.5194/gmd-2021-400. In review.
- Hunter, J. R., P. D. Craig, and H. E. Phillips. 1993. On the use of random walk models with spatially variable diffusivity. *J. Comput. Phys.* **106**: 366–376. doi:10.1016/S0021-9991(83)71114-9
- Janjic, Z. I., T. Black, M. Pyle, H.-Y. Chuang, E. Rogers, and G. Dimego. 2005. High Resolution Applications of the WRF NMM. *21st Conference on Weather Analysis and Forecasting/17th Conference on Numerical Weather Prediction*. 21.
- Lellouche, J.-M., E. Greiner, O. Le Galloudec, and others. 2018. Recent updates to the Copernicus Marine Service global ocean monitoring and forecasting real-time 1/12° high-resolution system. *Ocean Sci.* **14**: 1093–1126. doi:10.5194/os-14-1093-2018
- López, A. G., J. L. Wilkin, and J. C. Levin. 2020. Doppio-a ROMS (v3.6)-based circulation model for the Mid-Atlantic Bight and Gulf of Maine: Configuration and comparison to integrated coastal observing network observations. *Geosci. Model Dev.* **13**: 3709–3729. doi:10.5194/gmd-13-3709-2020
- Mesinger, F., G. DiMego, E. Kalnay, and others. 2006. North American regional reanalysis. *Bull. Am. Meteorol. Soc.* **87**: 343–360. doi:10.1175/BAMS-87-3-343
- North, E. W., Z. Schlag, R. R. Hood, M. Li, L. Zhong, T. Gross, and V. S. Kennedy. 2008. Vertical swimming behavior influences the dispersal of simulated oyster larvae in a coupled particle-tracking and hydrodynamic model of Chesapeake Bay. *Mar. Ecol. Prog. Ser.* **359**: 99–115. doi:10.3354/meps07317
- Ris, R. C., L. H. Holthuijsen, and N. Booij. 1999. A third-generation wave model for coastal regions: 2. Verification. *J. Geophys. Res. Ocean.* **104**: 7667–7681. doi:10.1029/1998JC900123
- Rubey, W. W. 1933. Settling velocity of gravel, sand, and silt particles. *Am. J. Sci.* **s5-25**: 325–338. doi:10.2475/ajs.s5-25.148.325
- Stacey, M. T., and D. K. Ralston. 2005. The scaling and structure of the estuarine bottom

- boundary layer. *J. Phys. Oceanogr.* **35**: 55–71. doi:10.1175/JPO-2672.1
- Taylor, G. I. 2002. Statistical theory of turbulence. *J. Plasma Fusion Res.* **78**: 773–781. doi:10.1585/jspf.78.773
- Tolman, H. L. 2002. User manual and system documentation of WAVEWATCH-III version 2.22. Tech. Note, US Dep. Commer. NOAA, NWS, NCEP, Washington, DC.
- Visser, A. W. 1997. Using random walk models to simulate the vertical distribution of particles in a turbulent water column. *Mar. Ecol. Prog. Ser.* **158**: 275–281. doi:10.3354/meps158275
- Voth, G. A., A. La Porta, A. M. Crawford, J. Alexander, and E. Bodenschatz. 2002. Measurement of particle accelerations in fully developed turbulence. *J. Fluid Mech.* **469**: 121–160. doi:10.1017/S0022112002001842
- Wilkin, J., and J. Levin. 2021. Outputs from a Regional Ocean Modeling System (ROMS) data assimilative reanalysis (version DopAnV2R3-ini2007) of ocean circulation in the Mid-Atlantic Bight and Gulf of Maine for 2007-2020. SEANOE. doi:10.17882/86286
- Wilkin, J., J. Levin, A. Lopez, E. Hunter, J. Zavala-Garay, and H. Arango. 2018. A Coastal Ocean Forecast System for U.S. Mid-Atlantic Bight and Gulf of Maine, p. 593–624. *In* E. Chassignet, A. Pascual, J. Tintoré, and J. Verron [eds.], *New Frontiers in Operational Oceanography*. GODAE OceanView.